200. Extraordinary Magnetic Flux Emergence Rate Preceding the May 2024 Extreme Geomagnetic Disturbances

Contributed by *Xudong Sun*. Posted on June 9, 2024

Xudong Sun[1], Aimee Norton[2], Shin Toriumi[3], Peter Schuck[4], Jie Zhang [5]
(1) Institute for Astronomy, University of Hawai'i at Mānoa, Makawao, HI, USA
(2) Hansen Experimental Physics Laboratory, Stanford University, Stanford, CA, USA
(3) Institute of Space and Astronautical Science, Japan Aerospace Exploration Agency, Sagamihara, Kanagawa, Japan
(4) Heliophysics Science Division, NASA Goddard Space Flight Center, Greenbelt, MD, USA
(5) Department of Physics and Astronomy, George Mason University, Fairfax, VA, USA

Summary: NOAA active regions 13664/8, the solar source region responsible for the May 2024 extreme geomagnetic disturbances that caused the largest geomagnetic storm since 2003, broke the record of magnetic flux emergence rate in the SDO era.

Our Sun is entering the maximum phase of activity cycle 25. In May 2024, the NOAA Active Region 13664 and 13668 complex (hereafter AR 13664/8) generated a series of major eruptions, including ten GOES X-class flares (Fig. 1(a)) and 14 major CMEs from May 8 to 14. The three successive halo CMEs occurred on May 8, through their interaction in the interplanetary space, produced a complex interplanetary ICME sequence with the presence of extraordinary southward magnetic field (>70 nT), ultimately resulting in the third most intense geomagnetic disturbance in half a century (Fig. 1(b)). The maximum Dst index was -412 nT, only behind the March 1989 Quebec blackout (-589 nT) and the November 2003 Halloween event (-422 nT). Aurorae were reported across the globe, with rare sightings in Florida and Hawai'i.

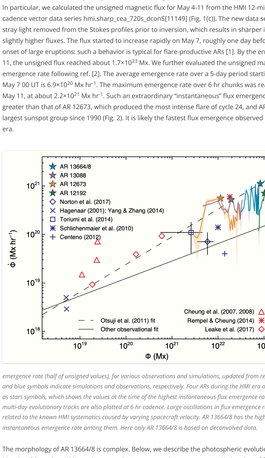

Figure 1 | Top: One-minute averaged GOES-18 soft X-ray (SXR) flux (0.1-0.8 nm band). The peak times of 10 GOES X-class flares associated with AR 13664/8 are noted by red ticks. Other X-class flares originated from AR 13663 in the northern hemisphere. The approximate Stonyhurst longitude of the AR central is noted at top. Middle: Hourly, real-time Dst index from World Data Center for Geomagnetism, Kyoto. Bottom: Mean unsigned magnetic flux of AR 13664/8 within 3-hour windows. The error bars show three times the standard deviation within the window.

We conducted a preliminary study of AR 13664/8 using photospheric observations from SDO/HMI. In particular, we calculated the unsigned magnetic flux for May 4-11 from the HMI 12-minute-cadence vector data series hmi.sharp_cea_720s_dconS[11149] (Fig. 1(c)). The new data series has stray light removed from the Stokes profiles prior to inversion, which results in sharper images and slightly higher flux values. The flux started to increase on May 7, roughly one day before the onset of large eruptions: such a behavior is typical for flare-productive ARs [1]. By the end of May 11, the unsigned flux reached about 1.7×10^{23} Mx. We further evaluated the unsigned magnetic flux emergence rate [2]. The average emergence rate over a 5-day period starting from May 7 00 UT is 6.9×10^{20} Mx hr^{-1}. The maximum emergence rate over 6 hr chunks was reached on May 11, at about 2.2×10^{21} Mx hr^{-1}. Such an extraordinary "instantaneous" flux emergence rate is greater than all of the AR 12673, which produced the most intense flare of cycle 24, and AR 12192, the largest sunspot group since 1990 (Fig. 2). It is likely the fastest flux emergence observed in the SDO era.

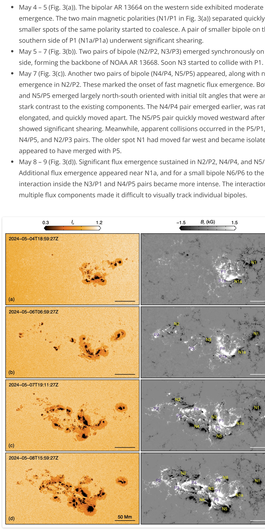

Figure 2 | Diagram of measured unsigned magnetic flux maximum signed flux emergence rate (Φ) vs. maximum signed flux (Φ) for various observations and simulations, updated from ref. [2]. Red and blue symbols indicate simulations and observations, respectively. Four ARs during the HMI era are included as stars symbols, which shows the values at the time of the highest instantaneous flux emergence rate. Their multi-day evolutionary tracks are also plotted at 6 hr cadence. Large oscillations in flux emergence rate may be related to the known HMI systematics caused by varying spacecraft velocity. AR 13664/8 has the highest instantaneous emergence rate among them. Here only AR 13664/8 is based on deconvolved data.

The morphology of AR 13664/8 is complex. Below, we describe the photospheric evolutions from May 4 to 8 based on HMI continuum and vector magnetic map sequence (Animation of Fig. 3). These descriptions are by no means comprehensive; rather, they are intended to guide the eyes of the readers. A movie of NOAA 13664/8 flux emergence is available.

- May 4 – 5 (Fig. 3(a)). The bipolar AR 13664 on the western side exhibited moderate flux emergence. The two main polarity regions (N1/P1 in Fig. 3(a)) separated quickly. Group of smaller spots of the same polarity started to coalesce. A pair of smaller bipole on the southern side of P1 (N1a/P1a) underwent significant shearing.
- May 5 – 7 (Fig. 3(b)). Two pairs of bipole (N2/P2, N3/P3) emerged synchronously on the eastern side, forming the backbone of NOAA AR 13668. Soon N3 started to collide with P1.
- May 7 (Fig. 3(c)). Another two pairs of bipole (N4/P4, N5/P5) appeared, along with new emergence in N2/P2. These marked the onset of fast magnetic flux emergence. Both N4/P4 and N5/P5 emerged largely north-south oriented with initial tilt angles that were anti-Hale, in stark contrast to the existing components. The N4/P4 pair emerged earlier, was rather elongated, and quickly moved apart. The N5/P5 pair quickly moved westward after birth and showed significant shearing. Meanwhile, apparent collisions occurred in the P5/P1, N3/P1, N4/P5, and N2/P3 pairs. The older spot N1 had moved far west and became isolated; p1a1 appeared to have merged with P5.
- May 8 – 9 (Fig. 3(d)). Significant flux emergence sustained in N2/P2, N4/P4, and N5/P5. Additional flux emergence appeared near N1a, and for a small bipole N6/P6 to the north. The interaction inside the N3/P1 and N4/P5 pairs became more intense. The interaction between multiple flux components made it difficult to visually track individual bipoles.

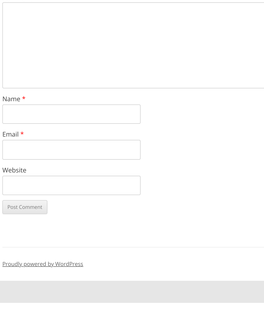

Figure 3 | Photospheric evolution of AR 13664/8. Four snapshots are shown for HMI continuum (left) and radial magnetic field (right) in Cylindrical Equal Area projection. The western portion in the first row was denoted as AR 13664 first, and the eastern portion as AR 13668 as it emerged. Pairs of bipoles are marked with N/P plus number for negative and positive polarities, respectively. A movie of NOAA 13664/8 flux emergence is available.

We emphasize that collisional and shearing motions between multiple bipoles were ubiquitous in AR 13664/8. This aspect, coined as "collisional shearing" between non-conjugate polarity pairs, was hypothesized to be crucial for producing intense eruptive activities as flux emergence [3]. Another interesting feature is the formation of δ-penumbrae: there area significantly increased as the bipole interactions intensified.

In addition to collisions, complex regions can be formed though 1) multi-loop buoyancy [4] and 2) deformation of flux tubes due to convective turbulence or a kink instability [4]. While we can infer (imperfectly) the subsurface geometry of the magnetic fields as the AR emerges, 13664/8 presents a challenge. The tilt angles of the emerging N4/P4 and N5/P5 bipoles are slightly anti-Hale and equal. They emerge within 24 hours of the N2/P2 and N3/P3 bipoles that emerge simultaneously with tilt angles obeying Hale and Joy's law. How two, multi-loop buoyancy events can happen co-spatially within 24 hours with bipolar tilt angles 180 degrees different from each other is puzzling. The emergence of flux from an O-ring or bubble could explain the observed geometry, with N2/P2 and N3/P3 emerging from the top of the O-ring first then N4/P4 and N5/P5 emerging from the bottom of the O-ring later.

References

[1] Toriumi, S., & Wang, H. 2019, *Living Rev. Sol. Phys.*, **16**, 3
[2] Sun, X., & Norton, A. A. 2017, *Res. Not. AAS*, **1**, 24
[3] Chintzoglou, G., Zhang, J., Cheung, M. C. M., & Kazachenko, M. 2019, *Astrophys. J.*, **871**, 67
[4] Toriumi, S., Schrijver, C. J., Harra, L. K., Hudson, H., & Nagashima, K. 2017, *Astrophys. J.*, **834**, 56
[5] Norton, A. A., Levens, P. J., Knizhnik, K. J., Linton, M. G., & Liu, Y., 2022, *Astrophys. J.*, **938**, 117

Posted in Magnetic Field, solar flares, sunspots . 513 views. Leave a comment

← Cycle 25: Timing of Polar field Reversal based on Advective Flux Transport Model

Leave a comment

Your email address will not be published. Required fields are marked *

Comment

Name *

Email *

Website

Post Comment

Search

RECENT COMMENTS

Muh. Khal on Solar Farside Magnetograms from...
darius on The STARA Sunspot Catalog
Martina smith! on Solar Farside Magnetograms from...
cindy on Solar Oblateness and Its...
Junwei Zhao on Computing Helioseismic Sensitivity Kernels...

ARCHIVES

June 2024 (1)
March 2024 (1)
February 2024 (1)
January 2024 (1)
September 2023 (3)
July 2023 (4)
October 2022 (4)
August 2022 (2)
July 2022 (2)
June 2022 (1)
May 2022 (2)
April 2022 (1)
March 2022 (3)
February 2022 (3)
November 2021 (3)
October 2021 (3)
September 2021 (3)
August 2021 (2)
June 2021 (3)
May 2021 (1)
April 2021 (2)
March 2021 (3)
January 2021 (4)
December 2020 (1)
November 2020 (1)
October 2020 (2)
September 2020 (2)
June 2020 (3)
May 2020 (1)
March 2020 (2)
February 2020 (3)
December 2019 (1)
October 2019 (2)
September 2019 (2)
August 2019 (1)
June 2019 (3)
April 2019 (2)
March 2019 (2)
February 2019 (2)
January 2019 (2)
December 2018 (1)
November 2018 (3)
September 2018 (5)
August 2018 (1)
July 2018 (3)
June 2018 (5)
May 2018 (2)
April 2018 (4)
March 2018 (7)
February 2018 (2)
January 2018 (3)
December 2017 (4)
November 2017 (3)
October 2017 (1)
September 2017 (1)
August 2017 (1)
July 2017 (1)
May 2017 (2)
March 2017 (1)
February 2017 (2)
December 2016 (1)
November 2016 (1)
October 2016 (2)
September 2016 (2)
August 2016 (2)
July 2016 (1)
June 2016 (2)
May 2016 (2)
April 2016 (3)
March 2016 (1)
January 2016 (1)
December 2015 (1)
November 2015 (1)
October 2015 (1)
September 2015 (1)
August 2015 (2)
July 2015 (1)
June 2015 (2)
May 2015 (1)
April 2015 (1)
February 2015 (1)
January 2015 (3)
November 2014 (1)
October 2014 (3)
September 2014 (2)
August 2014 (2)
July 2014 (2)
June 2014 (3)
May 2014 (6)
April 2014 (3)
March 2014 (3)
February 2014 (4)
January 2014 (3)

CATEGORIES

Helioseismology (65)
Machine Learning (7)
Magnetic Field (115)
Other (2)
solar convection (1)
solar cycles (15)
solar flares (14)
solar rotation (1)
solar-stellar connection (1)
solar-stellar connection (1)
sunspots (7)

TAGS

active region (4)
active regions (4)
CME (3)
convection (3)
coronal modeling (3)
dynamo (4)
eruption (3)
far-side imaging (3)
flare (3)
flare forecast (3)
flares (5)
flux (3)
flux cancellation (3)
helioseismic wave (3)
helioseismology (4)
machine learning (3)
magnetic field (5)
magnetic fields (3)
magnetic helicity (3)
magnetic reconnection (3)
meridional circulation (3)
meridional flow (4)
modelling (3)
penumbra (3)
polar field (3)
Python (3)
Rossby waves (3)
solar cycle (4)
solar cycles (5)
solar flares (3)
solar interior (3)
solar rotation (3)
subsurface flows (3)
surrounding sunspot (3)
sunspot oscillations (3)
sunspots (5)
supergranules (3)
synoptic maps (3)
time-distance (3)
tornadoes (3)
vector field (3)
vector magnetogram (3)
white-light flares (3)

META

Entries RSS
Comments RSS